Original Article

JCBFM

Journal of Cerebral Blood Flow & Metabolism
2016, Vol. 36(5) 928–940

DOI: 10.1177/0271678X16629482
jcbfm.sagepub.com
SAGE

Compartmentalised energy metabolism supporting glutamatergic neurotransmission in response to increased activity in the rat cerebral cortex: A ^{13}C MRS study *in vivo* at 14.1 T

Sarah Sonnay[1], João MN Duarte[1], Nathalie Just[2] and Rolf Gruetter[1,3,4]

Abstract

Many tissues exhibit metabolic compartmentation. In the brain, while there is no doubt on the importance of functional compartmentation between neurons and glial cells, there is still debate on the specific regulation of pathways of energy metabolism at different activity levels. Using ^{13}C magnetic resonance spectroscopy (MRS) *in vivo*, we determined fluxes of energy metabolism in the rat cortex under α-chloralose anaesthesia at rest and during electrical stimulation of the paws. Compared to resting metabolism, the stimulated rat cortex exhibited increased glutamate–glutamine cycle (+67 nmol/g/min, +95%, $P < 0.001$) and tricarboxylic (TCA) cycle rate in both neurons (+62 nmol/g/min, +12%, $P < 0.001$) and astrocytes (+68 nmol/g/min, +22%, $P = 0.072$). A minor, non-significant modification of the flux through pyruvate carboxylase was observed during stimulation (+5 nmol/g/min, +8%). Altogether, this increase in metabolism amounted to a 15% (67 nmol/g/min, $P < 0.001$) increase in $CMR_{glc(ox)}$, i.e. the oxidative fraction of the cerebral metabolic rate of glucose. In conclusion, stimulation of the glutamate–glutamine cycle under α-chloralose anaesthesia is associated to similar enhancement of neuronal and glial oxidative metabolism.

Keywords

Functional MRI (fMRI), glucose, energy metabolism, magnetic resonance, neuronal–glial interaction

Received 15 September 2015; Revised 15 December 2015; Accepted 6 January 2016

Introduction

Brain activity has important energy requirements that are satisfied by an efficient provision of oxygen and nutrients, principally glucose, supplied by increased local cerebral blood flow and volume. Changes in local brain activity are accompanied by concomitant modifications of local blood flow and glucose utilisation, which are the basis for functional mapping by blood oxygenation level-dependent (BOLD) functional magnetic resonance imaging (fMRI) and by positron emission tomography (PET) with radioactive glucose analogues, respectively. In the rat cortex, oxidative metabolism of glucose was demonstrated to increase upon enhanced brain activity during forepaw stimulation.[1] Moreover, Sibson et al.[2] reported that the rate of glutamate–glutamine cycle that depicts glutamatergic neurotransmission is coupled to glucose oxidation in the cortex (reviewed also by Hyder and Rothman[3]). However, these kinds of analyses are considered reductionist since they ascribe the neurotransmission-associated glucose oxidation exclusively to neurons, even though astrocytes have an active role in the

[1]Laboratory for Functional and Metabolic Imaging, École Polytechnique Fédérale, Lausanne, Switzerland
[2]Centre d'Imagerie Biomédicale – Animal and Technology Core, Lausanne, Switzerland
[3]Department of Radiology, University of Geneva, Switzerland
[4]Department of Radiology, University of Lausanne, Switzerland

Corresponding author:
João MN Duarte, Laboratory for Functional and Metabolic Imaging, École Polytechnique Fédérale, CH-1015 Lausanne, Switzerland.
Email: joao.duarte@epfl.ch

glutamate–glutamine cycle.[4] Indeed, although the link between cerebral activity and metabolic fluxes for production of energy has been suggested since early studies of brain energy metabolism, the effective contribution of glial oxidative metabolism to the support of neurotransmission *in vivo* is still unclear.[5]

Astrocytes are polarized cells linking synaptic activity to the vascular system: while fine perisynaptic processes engulf the synapses and are capable of regulating synaptic function, larger vascular processes that surround arterioles and capillaries are more specialized in nutrient uptake.[6] In addition, astrocytes are interconnected via gap junctions forming a complex functional network, and the astrocyte syncytium integrates surrounding signals, efficiently detects neuronal activity, transmits signals to neighbouring cells and regulates supply of energy substrates to neurons, thus bridging brain activity and hemodynamic responses.[7]

^{13}C MRS during administration of a ^{13}C-enriched substrate can distinguish ^{13}C isotope incorporation over time into different molecules and into specific carbon positions within one molecule.[8–10] The analysis of ^{13}C enrichment over time with mathematical models of energy metabolism that take in account the specificity of ^{13}C labelling through different metabolic pathways or reactions enable the effective distinction of contributions of neurons and astrocytes to brain oxidative metabolism.[8,9] In the present study, we tested the hypothesis that focal cortical activation results in enhanced neurotransmission rate, leading to increased rates of neuronal and glial oxidative metabolism.

Materials and methods

Animals

All experiments were performed in accordance with the Swiss federal law on animal experimentation and approved by the local authority (EXPANIM-SCAV) and are reported according to the ARRIVE guidelines. Male Sprague–Dawley rats ($n = 18$, 319 ± 19 g, from Charles River Laboratoires, France) were randomly allocated to experimental groups, and were prepared for MR experiments as previously detailed.[9,11] Briefly, rats were anesthetised with 2% isoflurane anaesthesia vaporized in 30% O_2 in air, were intubated and mechanically ventilated. Then, catheters were inserted into a femoral vein for infusion of phosphate-buffered saline solutions containing [1,6-^{13}C]glucose (Isotec, Sigma-Aldrich, Basel, Switzerland) or α-chloralose (Acros Organics, Geel, Belgium), and into a femoral artery for physiology monitoring and blood sampling. Heart rate, arterial blood pressure, body temperature and breathing rate were continuously monitored with an animal monitoring system (SA Instruments, Stony Brook, NY, USA). Arterial pH and pressures of CO_2 (P_aCO_2) and O_2 (P_aO_2) were measured using a blood gas analyser (AVL Compact 3, Roche Diagnostics, Rotkreuz, Switzerland), and were maintained at physiological levels by adjusting respiratory rate and volume. Body temperature was maintained at 37°C with a warm water circulation. Plasma glucose and lactate concentrations were quantified with the glucose or lactate oxidase methods, respectively, using two GM7 Micro-Stat analysers (Analox Instruments, London, UK). After positioning the animals in a home-built holder with ear and mouth inserts for stereotaxic fixation, anaesthesia was switched to α-chloralose (80 mg/kg bolus followed by a continuous intravenous infusion rate of 27 mg/kg/h). For ^{13}C MRS, [1,6-^{13}C]glucose was administered as previously described [9] to reach 70% of fractional enrichment (FE) in plasma within 5 min and throughout the whole experiment.

Electrical stimulation

Stainless steel electrodes were inserted between the second and third digits of both forepaws and in the Achilles tendon of both hindpaws. Electrical stimulation was performed by delivering square pulses (0.5 ms width) at constant current of 2.5 and 3 mA for the fore- and hindpaws, respectively, using the DS8000 stimulator coupled to the A365 and DLS100 stimulus isolators (World Precision Instruments, Stevenage, UK). The applied paradigm was (30 s ON − 10 s OFF) repeated for 4 h, with stimulation frequency switching between 2 and 3 Hz every 5 min. Three rats were used to confirm prolonged and localized BOLD response over the 4 h of electrical stimulation. In addition, cortical BOLD responses were confirmed in every rat prior to MRS experiments.

MR experiments in vivo

All experiments were performed on a 14.1 T/26 cm horizontal bore magnet (Magnex Scientific, Abingdon, UK), equipped with 12 cm gradients (400 mT/m in 120 μs) and interfaced to a Direct Drive console (Agilent Technologies, Palo Alto, CA, USA). A home-built ^{1}H quadrature transmit/receive coil was used for fMRI. For ^{13}C MRS, the coil consisted of a ^{1}H quadrature surface coil and a ^{13}C linearly polarized surface coil. The rat brain was placed at the isocenter of the magnet and T_2-weighted images were acquired for anatomical reference with a fast spin echo sequence with repetition time (TR) of 4 s and effective echo time (TE) of 40 ms. Shimming was performed with FAST(EST)MAP.[12]

The BOLD response was measured in six slices of 1 mm thickness using a single shot gradient echo (GE) – echo planar imaging (EPI) sequence with TR = 2.5 s, TE = 17 ms, field of view of $30 \times 30\,mm^2$, matrix size of 64×64, and bandwidth of 200–250 kHz.[13] Images were reconstructed using home-built software routines implemented in Matlab (The MathWorks, Natick, MA, USA) and analysed as previously described.[11] Briefly, after motion correction with SPM8 (Statistical Parametric Mapping, London, UK), activation maps were computed on a voxel-wise basis from the comparison between the experimental fMRI data and the applied stimulation paradigm for the first, middle or last 7 min of acquisition using STIMULATE.[14] Only clusters including at least three voxels were considered significant. No other correction or filtering methods were applied.

MRS experiments were performed under stimulation ($n = 7$) or at rest ($n = 8$) in a volume of interest (VOI) of 94 µL ($2.2 \times 8.5 \times 5\,mm^3$) localised in the cortex, corresponding to the area of activation assessed by fMRI. For determination of amino acid concentrations, localized ^{1}H MRS was performed with STEAM with TR = 4 s, TE = 2.8 ms, and mixing time (TM) of 20 ms. ^{13}C MRS was performed using semi-adiabatic distortionless enhancement by polarization transfer (DEPT) combined with 3D-ISIS ^{1}H localization.[10] Acquisition of ^{1}H and ^{13}C spectra was performed either at rest or during stimulation. Spectral analysis was performed using LCModel (Stephen Provencher Inc., Oakville, ON, Canada) for both ^{1}H and ^{13}C spectra.[15]

MRS in vitro

At the end of each ^{13}C MRS experiment, rats were euthanized using a focused microwave fixation device (Gerling Applied Engineering, Modesto, CA, USA) at 4 kW for 2.2 s. The portion of cortex corresponding to the MRS VOI was dissected. Cortical tissue and plasma samples were stored at −80°C until processing for determination of ^{13}C FE. Water soluble metabolites were extracted with 7% (v/v) perchloric acid. Then samples were dried, re-dissolved in ^2H_2O (99.9% ^{2}H, Sigma-Aldrich), and ^{1}H and ^{13}C spectra were acquired as previously described [16] on a DRX-600 spectrometer equipped with a 5-mm cryoprobe (Bruker BioSpin SA, Fallanden, Switzerland). FE in carbons of glutamate, glutamine and aspartate measured in cortical extracts served to scale ^{13}C curves measured *in vivo*.[17]

Metabolic modelling

Glucose transport and consumption were analysed by fitting both dynamic and steady-state MRS data with a reversible Michaelis–Menten model as detailed previously.[18] The model was firstly fitted to glucose concentrations measured at steady-state in cortex and plasma. The resulting apparent Michaelis constant of glucose transport K_t was then used in the analysis of dynamic ^{13}C curves, thus determining the apparent maximum transport rate (T_{max}) and the cerebral metabolic rate of glucose (CMR_{glc}). The mathematical model of energy metabolism with two compartments[9] was fitted to the group average ^{13}C enrichment curves of glucose C6, and all aliphatic carbons of glutamate, glutamine and aspartate, and allowed to determine fluxes through the apparent glutamatergic neurotransmission (i.e. glutamate–glutamine cycle, V_{NT}), neuronal and glial TCA cycles ($V_{TCA}{}^n$ and $V_{TCA}{}^g$), pyruvate carboxylase (V_{PC}), exchange between TCA cycle intermediates oxaloacetate and 2-oxoglutarate with the respective amino acids ($V_X{}^n$ in neurons and $V_X{}^g$ in glia), as well as dilution fluxes at the level of pyruvate (V_{in}), glial acetyl-CoA (V_{dil}) and glial glutamine ($V_{ex}{}^g$). Reliability of the fitted parameters was evaluated by Monte Carlo analysis.[9,17] Calculated fluxes included the glutamine synthetase rate ($V_{GS} = V_{NT} + V_{PC}$), the fraction of the glial TCA cycle that results in full oxidation of pyruvate ($V_g = V_{TCA}{}^g - V_{PC}$), and the rate of oxidative glucose metabolism, that is $CMR_{glc(ox)} = (V_{TCA}{}^n + V_{TCA}{}^g + V_{PC})/2$. Numerical procedures were performed in Matlab.

Statistics

All data are shown as mean ± SD. For metabolic fluxes, the SD was calculated from fitting a Gamma function to the histograms that resulted from at least 1000 Monte-Carlo simulations. Error propagation was taken into account in all calculations. Flux comparison between experimental groups was performed by permutation analysis with 2000 random permutations, followed by individual two-tailed Student *t*-tests. Reported *P*-values were subjected to corrections for multiple testing using the Holm-Bonferroni method.[19]

Results

We applied simultaneous electrical stimulation of both fore- and hindpaws with the paradigm (30 s ON − 10 s OFF) for 4 h, which resulted in a prolonged and localized BOLD response over the whole stimulation period, indicating persistent neuronal activation (Figure 1(a) and (b)). The underlying cortical area of activation encompassed primary somatosensory cortex of the fore- and hindlimb regions, as well as primary and secondary motor cortices (Figure 1(c)). The volume of interest for localized MRS encompassed activated areas of the cortex (Figure 1(d)).

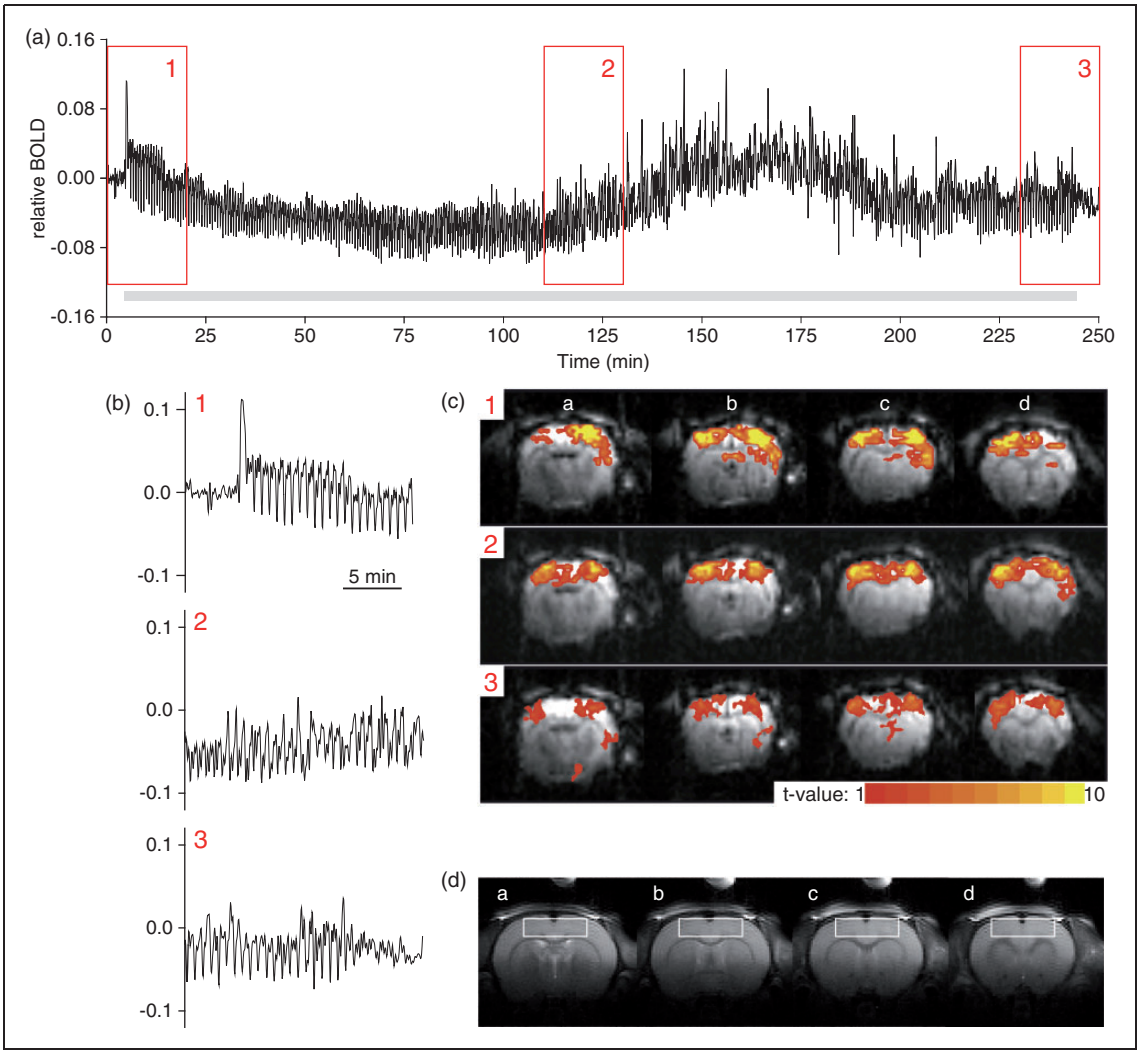

Figure 1. Prolonged and localized BOLD response in the rat cortex upon simultaneous electrical stimulation of both fore- and hindpaws was measured for 4 hours (a). The grey line represents the stimulation period. The three sections in red squares are expanded in (b), and the respective activation t-value maps are overlaid on GE-EPI images in (c) (a: bregma-1.8; b: bregma-0.8; c: bregma + 0.2; d: bregma + 1.2) after 7, 120 and 230 min. The paradigm was (30 s ON − 10 s OFF) repeated for 4 hours at constant current (2.5 and 3 mA for fore- and hindpaw, respectively) and variable frequency (2–3 Hz switched every 5 min). Panel (d) shows the respective T_2-weighted anatomical images with the typical position of the VOI for MRS ($2.2 \times 8.5 \times 5\,mm^3$). The sphere visible on the top of the rat brain is the ^{13}C formic acid reference used for radiofrequency pulse calibration.

To ensure tight physiology control over the course of the experiment, we measured arterial pH, P_aCO_2 and P_aO_2 which remained stable over the stimulation period (Table S1, Supplementary material). While arterial blood pressure was not modified throughout the experiment, heart rate continuously increased and was significantly higher (+11% at rest, +25% under stimulation) at the end of [1,6-^{13}C]glucose administration relative to prior infusion (Table S1, Supplementary material).

The administration of [1,6-^{13}C]glucose resulted in a rise of plasma substrate concentrations during the entire ^{13}C MRS experiment (Figure 2). FE of plasma glucose C1 rose within 5 min after starting the infusion of [1,6-^{13}C]glucose and remained stable thereafter. At the end of the experiment, FE of plasma glucose C1 was $63 \pm 4\%$ and $67 \pm 5\%$ for the resting and stimulated group, respectively (Figure 2(c)). FE of glucose C1 in the cortex was $63 \pm 6\%$ and $67 \pm 4\%$ for the resting and stimulated group, respectively, as determined from tissue extracts at the end of the experiment.

FE of lactate, alanine and acetate became enriched upon [1,6-^{13}C]glucose infusion (Figure 2(c)). At the end of the experiment, the FE of plasma lactate, alanine and acetate reached $35 \pm 3\%$, $30 \pm 23\%$ and $20 \pm 7\%$, respectively, in rats at rest. Upon stimulation, the FE of plasma lactate, alanine and acetate reached $38 \pm 4\%$,

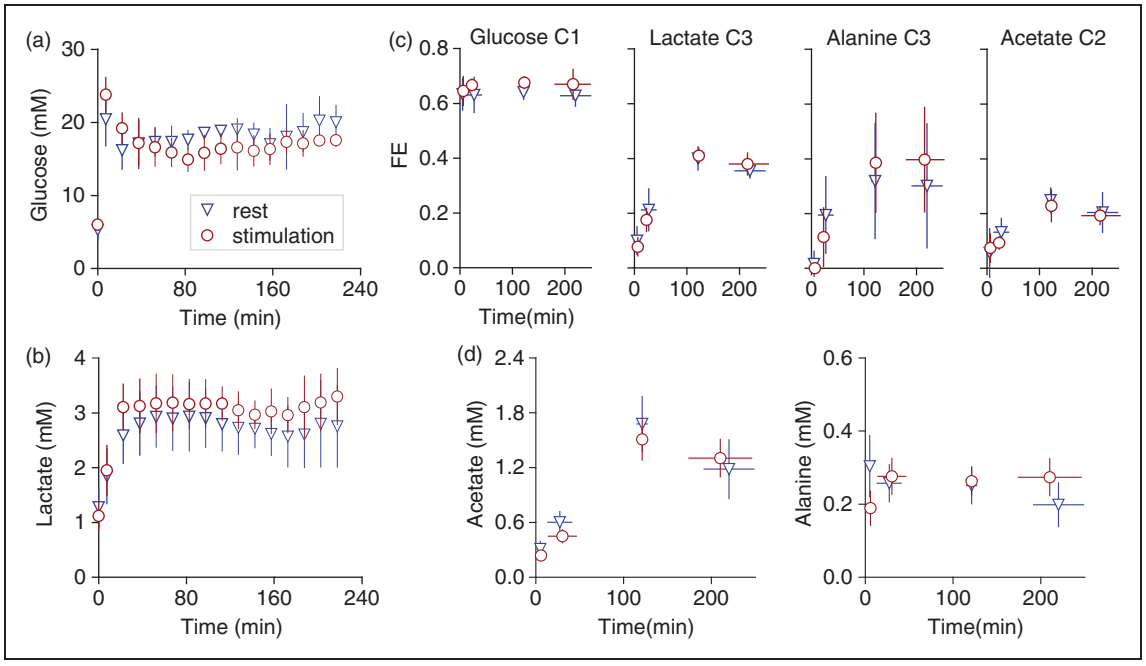

Figure 2. Plasma concentrations and ^{13}C enrichments of glucose and other possible substrates for brain metabolism. Plasma concentrations of glucose (a) and lactate (b) were measured enzymatically along the experiment *in vivo*. Fractional enrichment of glucose, lactate, alanine and acetate (c) and concentrations of alanine and acetate (d) were quantified in plasma extracts by MRS *in vitro*. Data from rats at rest ($n = 8$) and under stimulation ($n = 7$) are shown in blue triangles and red circles, respectively. Data are mean ± SD.

$40 \pm 20\%$ and $19 \pm 3\%$, respectively. Interestingly, FE of lactate and alanine were higher in the rat cortex than in plasma, but the opposite was found for acetate. FE of lactate, alanine and acetate in cortex extracts reached $43 \pm 14\%$, $46 \pm 6\%$ and $3 \pm 2\%$ at rest, and $47 \pm 11\%$, $50 \pm 5\%$ and $6 \pm 5\%$ upon stimulation, respectively.

We acquired ^{13}C spectra with a temporal resolution of 5.3 min. To increase the sensitivity in peak quantification, areas of carbon resonances from amino acids were measured using two averaged spectra, i.e. ~11 min of effective temporal resolution (Figure 3). The most prominent ^{13}C resonances observable in the rat cortex MRS were the C6 of glucose, the C4, C3 and C2 of glutamate and glutamine, and the C3 and C2 of aspartate (Figure 3).

To determine potential changes in glucose transport, we analysed both steady-state and dynamic glucose labelling and concentrations. Steady-state analysis of brain glucose transport using the plasma and brain glucose concentrations (Figure 4(a)) resulted in $K_t = 2.1 \pm 2.9$ mM at rest and 4.9 ± 2.3 mM under stimulation, which were then used as a constraint in dynamic modelling of ^{13}C curves (Figure 4(b)). Glucose curves were fitted only for the first hour of infusion because the largest glucose variations occur within the first 20 min after infusion onset. T_{max} and CMR_{glc} were, respectively, 2.4 ± 0.3 and 0.47 ± 0.05 µmol/g/min at rest and 2.6 ± 0.3 and 0.56 ± 0.07 µmol/g/min upon prolonged stimulation, respectively. The nominal variation of CMR_{glc} under stimulation (ΔCMR_{glc}) was 0.089 ± 0.090 µmol/g/min, representing a 19% increase in global glucose catabolism. Given the large uncertainty associated to K_t, we tested the effect of this parameter on the estimation of T_{max} and CMR_{glc} (Figure 4(c) and (d)). For the range of values tested, any variation in either T_{max} or CMR_{glc} was within their uncertainty.

The total concentrations of glutamate, glutamine and aspartate measured in the cortex were 10.1 ± 1.6, 4.9 ± 1.2 and 3.6 ± 0.8 µmol/g for rats at rest, and 11.2 ± 1.0, 6.1 ± 1.1 and 3.7 ± 0.6 µmol/g in rats under stimulation, respectively. These concentrations were used in the mathematical model. The two-compartment model of energy metabolism mimicked the measured turnover curves in both resting ($R^2 = 0.970$) and stimulation ($R^2 = 0.977$) conditions. Notably, metabolic fluxes were estimated in the rat cortex with excellent precision (Table S2, Supplementary material), despite the smaller VOI and lower temporal resolution of the measured ^{13}C enrichment curves, relative to previous ^{13}C MRS experiments in the whole rat brain.[9,17] At rest, the rate of glutamatergic neurotransmission, i.e. the glutamate–glutamine cycle (V_{NT}), was 0.070 ± 0.014 µmol/g/min and glutamine synthetase was 0.13 ± 0.02 µmol/g/min.

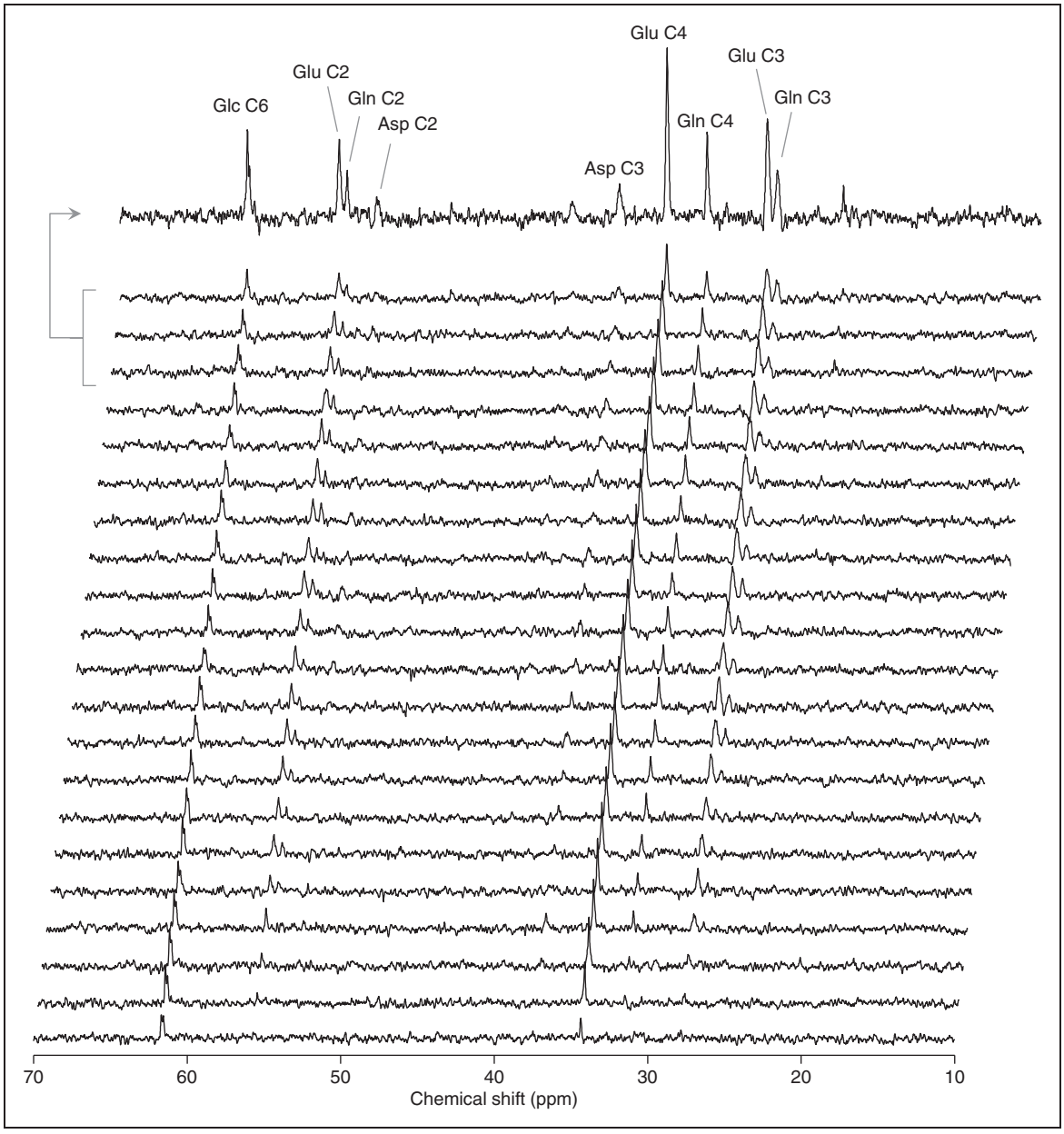

Figure 3. Typical ^{13}C spectra acquired at 14.1 T from a volume of 94 μL in the rat cortex during [1,6-^{13}C]glucose infusion. Spectra were summed with a temporal resolution of 11 min, and 7-Hz Lorentzian apodization was applied prior to Fourier transformation. The top spectrum is the sum of the spectra acquired for about 33 min starting 3.5 hours after the onset of [1,6-^{13}C]glucose infusion. Spectra are labelled as follows: Glc, glucose; Glu, glutamate; Gln, glutamine; Asp, aspartate.

The flux through the trycarboxylic acid cycle in neurons ($V_{TCA}{}^{n}$) and in astrocytes ($V_{TCA}{}^{g}$) were 0.53 ± 0.02 and 0.31 ± 0.04 μmol/g/min, respectively. $V_{TCA}{}^{g}$ was thus 37% of total glucose oxidative metabolism in the cortex, that is $CMR_{glc(ox)}$. Pyruvate carboxylation (V_{PC}) was 0.064 ± 0.006 μmol/g/min, representing 21% of $V_{TCA}{}^{g}$. The oxidative fraction of the cerebral metabolic rate of glucose, called $CMR_{glc(ox)}$, was 0.45 ± 0.02 μmol/g/min, and there was a net efflux of pyruvate (most likely in the form of lactate) from the cortex ($V_{out} - V_{in}$) of 0.035 ± 0.084 μmol/g/min.

To determine the effect of stimulation on the aforementioned metabolic fluxes, the experiment was repeated in rats submitted to the stimulation protocol shown to result in persistent cortical activation (Figure 1). Under stimulation, the rat cortex showed faster neurotransmission rate, i.e. faster glutamate–glutamine cycle, and faster neuronal and glial oxidative

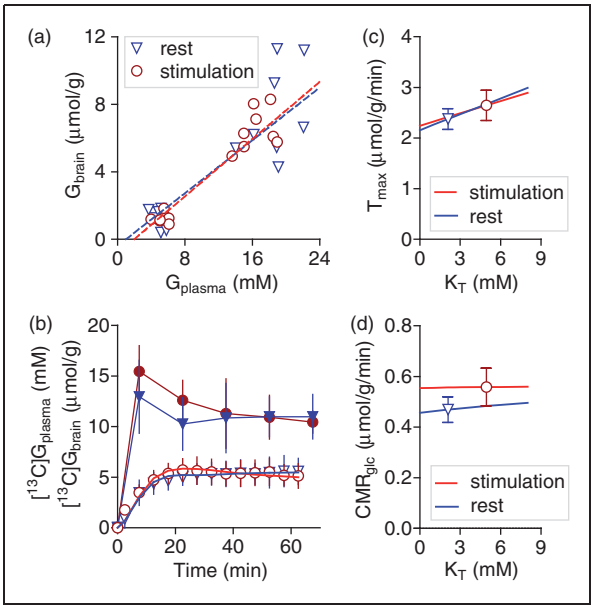

Figure 4. Brain glucose content and enrichment described by the reversible Michaelis–Menten model of glucose transport. (a) Analysis of brain glucose transport using steady-state plasma and brain glucose concentrations (G_{plasma} and G_{brain}, respectively) measured before [1,6-^{13}C]glucose infusion and when G_{plasma} was stable for at least 1 h. Red and blue lines represent the fit to data acquired under stimulation (circles) and resting (triangles), respectively. Panel (b) shows [^{13}C]G_{brain} and [^{13}C]G_{plasma} over 50 min and the best fit of the dynamic model. Data from rats at rest ($n = 8$) and under stimulation ($n = 7$) are shown in blue triangles and red circles, respectively. Filled and open symbols in (b) indicate [^{13}C]G_{plasma} (in mM) and [^{13}C]G_{brain} (in µmol/g), respectively. The effect of K_t on the determination of T_{max} and CMR_{glc} is shown in (c) and (d), respectively. Data are mean ± SD.

metabolism, compared to the cortex at rest (Figure 5, Table S2, Supplementary material). More precisely, intermittent focal cortical activity resulted in an increase in V_{NT} ($\Delta V_{NT} = 0.067 \pm 0.031$ µmol/g/min, +95%, $P < 0.001$), V_{GS} ($\Delta V_{GS} = 0.072 \pm 0.033$ µmol/g/min, +53%, $P < 0.001$), and $V_{TCA}{}^{n}$ ($\Delta V_{TCA}{}^{n} = 0.062 \pm 0.036$ µmol/g/min, +12%, $P < 0.001$). The increase in the astrocytic TCA cycle rate was substantial but within the uncertainty of its estimation ($\Delta V_{TCA}{}^{g} = 0.068 \pm 0.112$ µmol/g/min, +22%, $P = 0.072$). The fraction of $V_{TCA}{}^{g}$ that represents full oxidation of pyruvate increased by 26% ($\Delta V_{g} = 0.063 \pm 0.112$ µmol/g/min, $P = 0.226$). The flux through pyruvate carboxylase was similar at rest and during stimulation, with an increase in V_{PC} that was one order of magnitude smaller than that in fluxes of oxidative metabolism ($\Delta V_{PC} = 0.005 \pm 0.012$ µmol/g/min, +8%). Upon stimulation, V_{PC} was 18% of $V_{TCA}{}^{g}$ that in turn represented 39% of $CMR_{glc(ox)}$. The variation in the oxidative fraction of CMR_{glc} upon stimulation matched ΔV_{NT}, namely $\Delta CMR_{glc(ox)}$ was 0.067 ± 0.059 µmol/g/min (an increase of +15%, $P < 0.001$). Interestingly, the dilution rates at the level of pyruvate were reduced upon stimulation, when compared to rest. Namely, ΔV_{in} and ΔV_{out} were -0.083 ± 0.037 and -0.039 ± 0.157 µmol/g/min, respectively.

Discussion

This study quantifies for the first time the effective magnitude of modifications in neuronal and glial oxidative metabolism induced by increased glutamate–glutamine cycling upon sensorial stimulation in the living brain, using ^{13}C MRS *in vivo*. The present results show that each molecule of glutamate that is released and converted to glutamine requires oxidation of one molecule of glucose, and demonstrated that enhancement of cortical activity *in vivo* is accompanied by stimulation of both neuronal and glial oxidative metabolism under α-chloralose anaesthesia, with substantial activity-linked glucose oxidation occurring in glia.

Modifications of cortical metabolism were determined upon sensorial stimulation over 4 hours. The four paws of the rat were electrically stimulated with a paradigm that included 10 s of rest after each 30 s of current delivery. Such stimulation circumvented the loss of signal in BOLD fMRI upon continuous electrical stimulation,[11] and prolonged and localized BOLD response following the applied paradigm was detected over the entire stimulation period (4 hours) in the cortex. A volume of interest of 94 µL was placed in the area of intense cortical activation that encompassed primary somatosensory cortex of the fore- and hind limb regions, as well as primary and secondary motor areas. Direct detection of ^{13}C enrichment of aliphatic carbons of glutamate, glutamine and aspartate from this small volume provided sufficient temporal resolution to determine fluxes of energy metabolism in neurons and astrocytes, as well as the rate of the glutamate–glutamine cycle, as in previous studies that investigated the whole rat brain.[9,17]

^{13}C MRS studies *in vivo* of amino acid turnover upon stimulus-induced brain activation have been mostly performed using ^{1}H[^{13}C] MRS, i.e. indirect detection of signals from ^{13}C-coupled protons.[1,20,21] Although high sensitivity can be achieved with ^{1}H[^{13}C] MRS *in vivo*, the lower spectral resolution hampers an analysis of carbon positions C3 and C2 of glutamate and glutamine, restricting therefore the reliability and the number of fluxes being determined. In the particular, a number of assumptions had to be made on the glial fluxes V_{PC} and $V_{TCA}{}^{g}$ (discussed by Lanz et al.[5]). Nevertheless, increased oxidative metabolism and CMR_{glc} were determined upon forepaw stimulation in rats[1,20] and during intense cortical

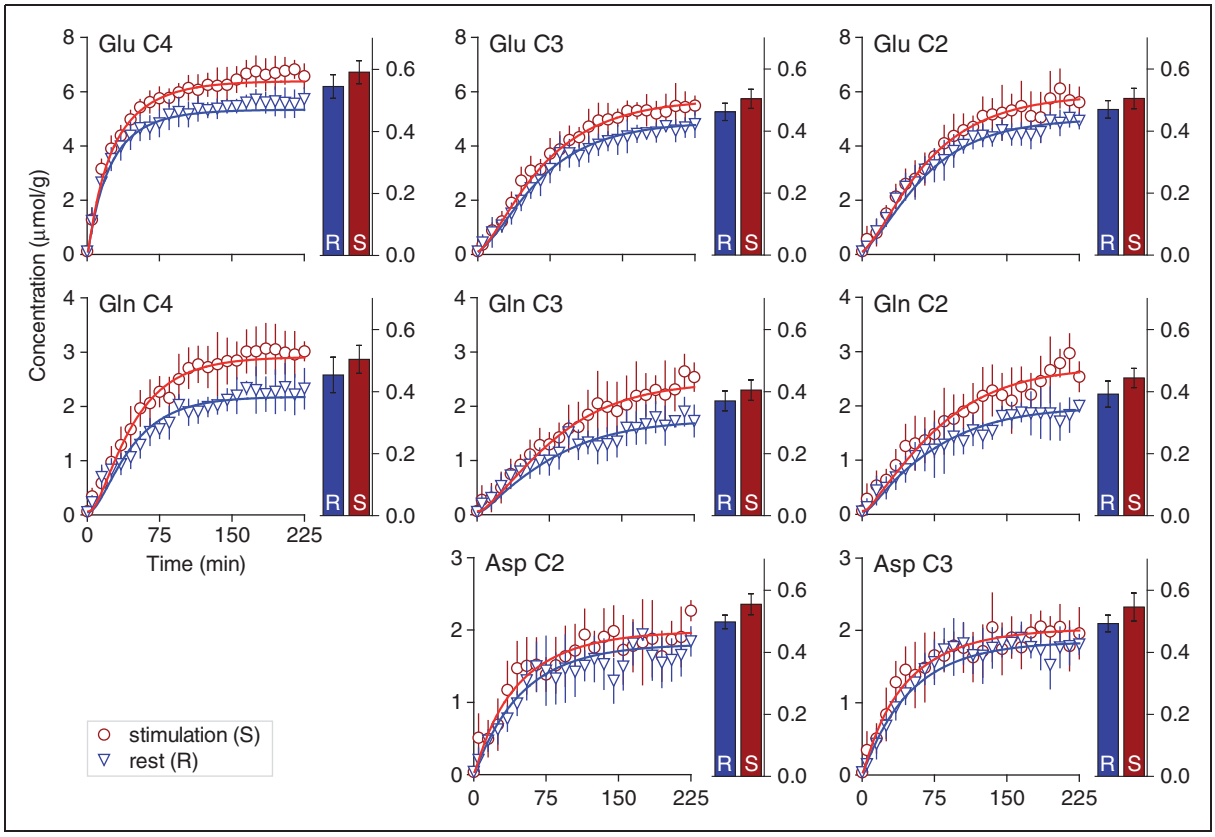

Figure 5. Average ^{13}C enrichment curves (in μmol/g) of aliphatic carbons of glutamate (Glu), glutamine (Gln) and aspartate (Asp) measured in the rat cortex at rest and during stimulation, and best fit of the two-compartment model of brain energy metabolism. The bar graphs on the right of each experimental curve represents the FE of the respective carbon as measured in cortical extracts. Data from rats at rest (R, $n = 8$) and under stimulation (S, $n = 7$) are shown as blue triangles and red circles, respectively. Data are mean ± SD.

activity induced by bicuculline.[21] In contrast, the analysis in the present study was performed with minimal assumptions on metabolic fluxes leading to the labelling of measured amino acids.

It is important to note that the stimulation paradigm includes a small 10-s interruption after each 30 s of stimulus delivery, which results in cyclic changes in brain function (activation and deactivation). These inter-stimulus intervals allowed observing a BOLD effect that persisted over four hours. However, under such a stimulation protocol, the cortical metabolism is not in a stationary state, as assumed in the mathematical model of brain metabolism that was employed to determine metabolic fluxes. Nevertheless, we assumed that cortical metabolism was at a *quasi*-steady-state and that this approximation does not preclude the present mathematical analysis of ^{13}C incorporation into amino acids. Moreover, in this study, we observed a slight increase in the heart rate during the ^{13}C MRS experiment (Table S1, Supplementary material), suggesting that there may be a reduction in anaesthesia depth. Although brain activity and metabolism may have varied while measuring ^{13}C enrichment of amino acids, most information for the metabolic flux analysis lies in the early fast rise of ^{13}C incorporation, and may be little affected by a slow reduction in anaesthesia depth over the whole experimental protocol.

Coupling between oxidative metabolism and glutamatergic neurotransmission

Many studies provided evidence of a direct link between the BOLD response and neuronal activity.[22,23] In addition, the complex astrocytic network has influence on the hemodynamic response associated to the neurovascular (i.e. increased local cerebral blood flow) and neurometabolic (i.e. local changes in blood oxygen and glucose delivery and metabolism to fulfil energy demand) coupling, and modulates synaptic events.[7,24–26] Therefore, a synchronized and cooperative interaction between neurons and glia orchestrates the hemodynamic response to fulfil the energy demand associated to neurotransmission. Studies using PET, autoradiography and ^{13}C MRS have reported increased overall cerebral glucose consumption (CMR_{glc}) with increased cerebral activity, which may be driven by

stimulation of both glial and neuronal oxidative metabolism.[3–5]

In the present ^{13}C MRS experiments, glucose administration was a hyperglycaemic clamp that ensured stable glucose enrichment in plasma. In such conditions, glucose transport was assessed to be unaltered by increased cortical activity (similar T_{max} and K_t). In contrast, CMR_{glc} was increased during stimulation relative to rest, which resulted in increased glucose utilization relative to transport capacity in the stimulated condition. This resulted in a smaller T_{max}/CMR_{glc} during stimulation compared to rest, which is consistent with activity-induced reduction in levels of glucose measured by ^{1}H MRS in humans[27] and animals.[13]

Focal cortical activity resulted in a 95% increase in V_{NT} and 15% increase in $CMR_{glc(ox)}$, with $\Delta CMR_{glc(ox)}/\Delta V_{NT} \sim 1$, in line with the relationship often observed between glutamate release and glucose consumption.[3] Moreover, oxidative metabolism in astrocytes ($V_{TCA}{}^{g} = V_g + V_{PC}$) contributed to more than one-third of total oxidative metabolism, namely 38%, similar to determinations in the whole rat brain.[9,17] The stimulation-induced 26% increase in V_g (and thus a 22% increase in $V_{TCA}{}^{g}$) indicates an activation of glial oxidative metabolism by glutamate transmission, which is supported by the fact that astrocytic respiration is stimulated by glutamate.[28] In line with this, acoustic stimulation enhanced astrocytic oxidative metabolism in auditory structures of the awake rat brain, as probed with [2-^{14}C]acetate that is specifically taken by glial cells.[29] Photic stimulation in rats was also shown to induce [2-^{14}C]acetate uptake in the superior colliculus.[30] Interestingly, the authors further reported that acetate utilisation was much lower than CMR_{glc} and irresponsive to the stimulus rate, while CMR_{glc} showed a proportional response. The contrasting large metabolic response of astrocytes that we observed may in part reflect the fact that our study was performed under α-chloralose anaesthesia.

The mathematical model used implies that glial-specific pyruvate carboxylation leads to net formation of glutamate and eventually glutamine that is lost through V_{efflux} (Figure 6). For that, one molecule of glucose is split in two molecules of pyruvate to form oxaloacetate and acetyl-CoA. Thus, each molecule of glutamine synthetized from glucose via pyruvate carboxylase is associated with the generation of 2 ATP and 2 NADH by glycolysis and then consumption of one ATP by pyruvate carboxylase and generation of 2 NADH by pyruvate dehydrogenase and isocitrate dehydrogenase. Altogether, assuming a P:O ratio of 2.5, 11 ATP are produced in the generation *de novo* of one molecule of 2-oxoglutarate, which can be converted to glutamate and then glutamine. Thus, *de novo* glutamine synthesis in astrocytes could be a favourable pathway to produce energy for glutamine synthetase and for extrusion of the Na^+ that is co-transported upon glutamate removal from the extracellular space. V_{PC} was determined higher in the brain of awake than anaesthetised rats.[31] It is of interest to note that glutamate, whose concentration increases upon cortical stimulation *in vivo*,[13,27,32,33] can stimulate pyruvate carboxylation in mitochondria isolated from the rat brain.[34] On the other hand, glutamate can be oxidized to replenish TCA cycle intermediates, namely fumarate, oxaloacetate, malate and succinate that inhibit pyruvate carboxylation.[34] Moreover, local ADP to ATP ratio may increase during cortical stimulation, and ADP is also capable of inhibiting pyruvate carboxylase activity.[35] Regulation of pyruvate carboxylation is complex in the cellular context. In cultured astrocytes, K^+ elevations can stimulate CO_2 fixation[36] and glutamate was found to inhibit pyruvate carboxylation and glucose utilisation.[37] However, V_{PC} was reported unaltered during bicuculline-induced seizures under halothane anaesthesia.[38] Somatosensory stimulation did not cause a substantial increase in V_{PC} in the rat cortex under α-chloralose anaesthesia in the present study. For example, the small variation observed in net glutamate formation would only generate +55 nmol/g/min of ATP ($11 \times \Delta V_{PC}$) which is less than half of that required by the glutamate–glutamine cycle ($2 \times \Delta V_{NT} \sim 0.13$ μmol/g/min).

In contrast, the oxidation of glutamate could fuel its own uptake and glutamine synthesis.[4] Indeed, rather than loss of five carbon molecules (via $V_{efflux} = V_{PC}$), glutamate shunting through the TCA cycle with subsequent oxidation to oxaloacetate and subsequent condensation with acetyl-CoA (consuming ½ glucose) to generate 2-oxoglutarate would produce 16 ATP (effectively produced 4 NADH, 1 $FADH_2$ and 1 GTP, plus 1 NADH and 1 ATP from glycolysis) rather than the 11 ATP resulting from the *de novo* synthesis of 2-oxoglutarate using a full glucose molecule. Although not explicitly depicted in the model, glutamate oxidation and transference of ^{13}C labelling from glutamate to oxaloacetate is possible in both neurons and glia through mitochondrial exchange fluxes (V_X). Shunting a fraction of glutamate through the TCA cycle can effectively reduce the amount of glucose that is consumed to maintain the increased TCA cycle rate in astrocytes, and is consistent with the absence of a substantial stimulation-induced increase in V_{PC}. It is of interest to note in this context that increased neuronal activity has been reported to recruit mitochondria in astrocytic processes to approach sites of glutamate uptake,[39] thus likely facilitating its oxidation.

Nevertheless, the bulk of the cellular energy is derived from near-complete glucose oxidation, with one molecule of glucose oxidized ultimately generating

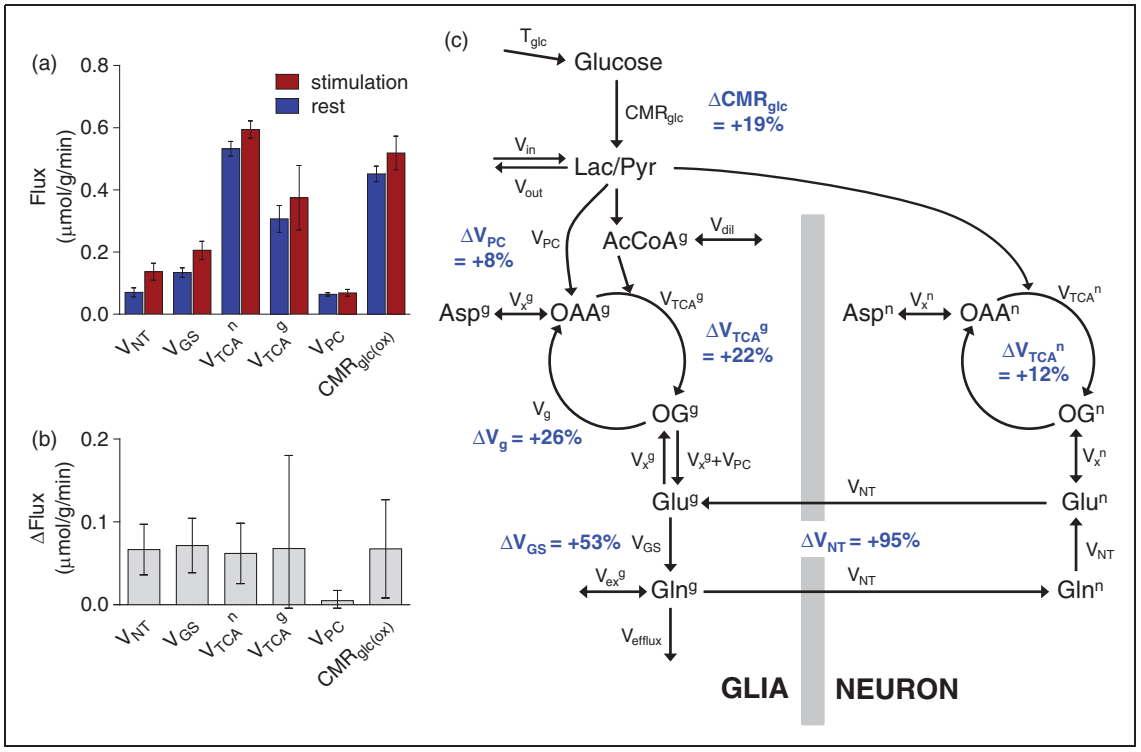

Figure 6. Modification of metabolic fluxes in the rat cortex during stimulation, relative to the resting state. Fluxes (a) and flux variation (b, ΔFlux) are shown with associated SD. The scheme in (c) shows the variation of the respective fluxes (text in blue) in the two-compartment model (for details see Duarte et al.[9]) that was adapted to include a dilution flux at the level of glial glutamine (V_{ex}^{g}, Gruetter et al.[8]). Glucose transport and consumption are represented by T_{glc} and CMR_{glc}, respectively. Pyruvate (Pyr) and lactate (Lac) are diluted with unlabelled substrates through V_{out}/V_{in}. V_{TCA}^{n} is the neuronal TCA cycle, $V_{TCA}^{g} = V_g + V_{PC}$ is the total glial TCA cycle, V_{PC} is the rate of pyruvate carboxylase. In the glial compartment, the dilution of label at the level of acetyl-CoA (AcCoA) by glial specific substrates is accounted by V_{dil}. TCA cycle intermediates oxaloacetate (OAA) and 2-oxoglutarate (OG) exchange with amino acids through the exchange flux V_X. V_{NT} and V_{GS} represent the glutamate–glutamine cycle and glutamine synthetase rates, respectively. Net efflux from the metabolic system occurs through the rate of glial glutamine loss V_{efflux}. The superscripts ^{g} and ^{n} distinguish metabolic pools or fluxes in the glial or neuronal compartment, respectively.

about 32 molecules of ATP (taking into account mitochondrial transport and assuming a P:O ratio of 2.5). Thus, glucose oxidation by the 26% stimulation-induced increase in V_g can produce about +1 µmol/g/min of ATP ($16 \times \Delta V_g$) that is similar to that produced in neurons and in excess of the increase in ATP required by the glutamate–glutamine cycle. Note, however, that astrocytes perform a substantial amount of work in regulating synaptic activity well beyond maintaining the glutamate–glutamine cycle and associated ion gradients: namely releasing transmitter molecules and neuromodulators that feedback to neurons and/or act on glial and blood vessel cells, to achieve a concerted modulation of synaptic activity, neuronal synchronisation and blood flow.[7,25,26]

In our model, labelling from intermediates of the TCA cycles into glutamate and *vice versa* are transferred via mitochondrial exchange fluxes (V_X^{n} and V_X^{g}) that have been proposed to represent the malate-aspartate shuttle.[8] A reliable estimation of these fluxes require that the initial data points of the ^{13}C curves of the amino acids are measured with good sensitivity.[5] Labelling of amino acids was measured in a VOI much smaller than in previous studies,[9,17] and thus with less sensitivity, which hampered the determination of V_X^{n} and V_X^{g}. Nevertheless, the larger uncertainty of V_X^{n} and V_X^{g} does not preclude the estimation of the remaining fluxes of the model.

Concentrations of amino acids determined in the cortex were slightly different in resting and stimulated rats. Moreover, there are reports of changes in cortical levels of glutamate, glutamine and aspartate upon focal activation.[13,40] Therefore, we tested the effect of amino acid concentrations (Figure S1, Supplementary material) and their distribution in the two compartments (Figure S2, Supplementary material) on the estimation of metabolic fluxes. Glutamate and glutamine levels affected V_{TCA}^{n} and V_{TCA}^{g}, respectively. For example, while more glutamate resulted in faster V_{TCA}^{n}, more glutamine resulted in faster V_{TCA}^{g}. Importantly, the

relative amount of glutamate in the neuronal and glial compartment also appears to be determinant for the absolute estimation of these fluxes. However, any putative effect of the brain's activity state on the relative distribution of the amino acids in the two cell types in the living brain has not been reported.

Stimulatory effects of activation on pathways fuelling glutamatergic neurotransmission in awake and anaesthetised subjects may not be equivalent. Moreover, there may be anaesthesia-specific effects on metabolic regulation. It is possible that flexible and independent adjustments of oxidative and glycolytic pathways occur in neurons and astrocytes, thus matching the cell-specific energy requirements of the cortical functional state. This study was conducted under α-chloralose anaesthesia, thus care should be taken when transposing these results to other anaesthesia conditions or the awake state.

Dilution of pyruvate and acetyl-CoA pools by unlabelled substrates

The two-compartment model employed for flux estimation includes dilution fluxes that represent either utilisation of unlabelled substrates that generate pyruvate (V_{in}) or pyruvate loss from the metabolic system (V_{out}),[9] whose fate is unknown, but probably mainly represents formation of lactate and subsequent release from the cortical parenchyma. In both functional states, the results indicated a net release of three carbon molecules from glycolysis ($V_{in} < V_{out}$). Moreover, stimulation caused a reduction in both fluxes, which was larger for V_{in} than V_{out} suggesting a further increased lactate release.[41] Loss of labelling also occurs via the pentose phosphate pathway. Conversely, diffusion of glycolytic intermediates through gap-junctions is of minor importance because metabolites in other brain areas (namely adjacent to the VOI) become equally enriched.

The present analysis of cortical metabolism did not consider the role of glycogen in supporting energy supply during stimulation. Glycogen content is stable in the resting brain but glycogenolysis may increase upon somatosensory stimulation.[42,43] The importance of glycogen metabolism in supporting glutamatergic transmission was demonstrated in cell cultures[44] and *in vivo*.[45] Increased glycogenolysis during cortical stimulation would lead to eventual dilution of the labelling in pools of pyruvate (taken in account by V_{in} in the model) as well as lactate, because of the equilibrative nature of lactate dehydrogenase.[41] At the end of the ^{13}C MRS experiment, the FE of glucose in cortical extracts was the same as that observed in plasma for both experimental conditions, and similarly the FE ratio of lactate C3 to glucose C1 was 0.68 ± 0.23 and 0.70 ± 0.16 at rest and after 4 h of stimulation, respectively. This suggests that even though glycogen may be a relevant energy buffer contributing to the generation of unlabelled pyruvate molecules, eventual modification of glycogenolysis rate during stimulation did not interfere with estimation of fluxes of oxidative metabolism in the present experiments, in which glucose was plentifully available from the blood stream.

In the model, V_{dil} is another dilution factor that specifically allows for dilution of glial acetyl-CoA.[9] While this flux was undetectable in the cortex of rats at rest, it was 0.14 μmol/g/min under stimulation, which is still substantially lower than values measured for the whole rat brain under identical experimental conditions.[9,17] Nevertheless, it suggests eventual oxidative utilization of glial-specific substrates upon stimulation, namely acetate[29,30] that increased in plasma with the hyperglycaemic clamp and had low FE (one-third of that in glucose and one half of that in lactate). Because FE of acetate in the cortex was much lower than in plasma, deacetylation reactions could also be a source of unlabelled acetyl-CoA in the brain.

Conclusion

Energy metabolism in astrocytes responds to increased brain activity, namely with increased mitochondrial oxidation to produce energy for supporting the glutamatergic transmission process. Despite being within the experimental error, the observed variation of $V_{TCA}{}^{g}$ suggests that the stimulation-induced enhancement of glucose oxidation in astrocytes can be as large as that in neurons.

Funding

This work was supported by the Swiss National Science Foundation (grant 148250 to JMND, and 149983 to RG) and by the CIBM of the EPFL, UNIL, UNIGE, HUG, CHUV and the Leenaards and Jeantet Foundations. SS was supported by the National Competence Center in Biomedical Imaging (NCCBI).

Acknowledgement

The authors thank Jaquelina Romero, Corina Berset and Anne-Catherine Clerc for the technical support.

Declaration of conflicting interests

The author(s) declared no potential conflicts of interest with respect to the research, authorship, and/or publication of this article.

Authors' contributions

RG initiated the project. JMND conceived and designed the experiments. SS performed the experiments. SS, NJ and JMND analysed the data. SS and JD wrote the manuscript.

NJ and RG contributed to the discussion and revised the manuscript.

Supplementary material

Supplementary material for this paper can be found at http://jcbfm.sagepub.com/content/by/supplemental-data

References

1. Hyder F, Chase JR, et al. Increased tricarboxylic acid cycle flux in rat brain during forepaw stimulation detected with $^{1}H[^{13}C]$NMR. *Proc Natl Acad Sci U S A* 1996; 93: 7612–7617.
2. Sibson NR, Dhankhar A, et al. Stoichiometric coupling of brain glucose metabolism and glutamatergic neuronal activity. *Proc Natl Acad Sci U S A* 1998; 95: 316–321.
3. Hyder F and Rothman DL. Quantitative fMRI and oxidative neuroenergetics. *Neuroimage* 2012; 62: 985–994.
4. Hertz L, Peng L and Dienel GA. Energy metabolism in astrocytes: High rate of oxidative metabolism and spatiotemporal dependence on glycolysis/glycogennolysis. *J Cereb Blood Flow Metab* 2007; 27: 219–249.
5. Lanz B, Gruetter R and Duarte JMN. Metabolic flux and compartmentation analysis in the brain *in vivo*. *Front Endocrinol (Lausanne)* 2013; 4: 156.
6. Iadecola C and Nedergaard M. Glial regulation of the cerebral microvasculature. *Nat Neurosci* 2007; 10: 1369–1376.
7. Cheung G, Chever O and Rouach N. Connexons and pannexons: newcomers in neurophysiology. *Front Cell Neurosci* 2014; 8: 348.
8. Gruetter R, Seaquist ER and Ugurbil K. A mathematical model of compartmentalized neurotransmitter metabolism in the human brain. *Am J Physiol Endocrinol Metab* 2001; 281: E100–E112.
9. Duarte JMN, Lanz B and Gruetter R. Compartmentalized cerebral metabolism of [1,6-^{13}C]glucose determined by *in vivo* ^{13}C NMR spectroscopy at 14.1 T. *Front Neuroenergetics* 2011; 3: 3.
10. Henry PG, Tkác I and Gruetter R. ^{1}H-localized broadband ^{13}C NMR spectroscopy of the rat brain *in vivo* at 9.4 T. *Magn Reson Med* 2003; 50: 684–692.
11. Sonnay S, Just N, et al. Imaging of prolonged BOLD response in somatosensory cortex of the rat. *NMR Biomed* 2015; 28: 414–421.
12. Gruetter R and Tkác I. Field mapping without reference scan using asymmetric echo-planar techniques. *Magn Reson Med* 2000; 43: 319–323.
13. Just N, Xin L, et al. Characterization of sustained BOLD activation in the rat barrel cortex and neurochemical consequences. *Neuroimage* 2013; 74: 343–351.
14. Strupp JP. Stimulate a GUI based fMRI analysis software package. *Neuroimage* 1996; 3: S607.
15. Henry PG, Oz G, et al. Toward dynamic isotopomer analysis in the rat brain *in vivo*: automatic quantitation of ^{13}C NMR spectra using LCModel. *NMR Biomed* 2003; 16: 400–412.
16. Duarte JMN, Cunha RA and Carvalho RA. Different metabolism of glutamatergic and GABAergic compartments in superfused hippocampal slices characterized by nuclear magnetic resonance spectroscopy. *Neuroscience* 2007; 144: 1305–1313.
17. Duarte JMN and Gruetter R. Glutamatergic and GABAergic energy metabolism measured in the rat brain by ^{13}C NMR spectroscopy at 14.1 T. *J Neurochem* 2013; 126: 579–590.
18. Duarte JMN and Gruetter R. Characterization of cerebral glucose dynamics *in vivo* with a four-state conformational model of transport at the blood-brain barrier. *J Neurochem* 2012; 121: 396–406.
19. Holm S. A simple sequentially rejective multiple test procedure. *Scand J Stat* 1979; 6: 65–70.
20. Hyder F, Rothman DL, et al. Oxidative glucose metabolism in rat brain during single forepaw stimulation: a spatially localized $^{1}H[^{13}C]$ nuclear magnetic resonance study. *J Cereb Blood Flow Metab* 1997; 17: 1040–1047.
21. Patel AB, de Graaf RA, et al. Glutamatergic neurotransmission and neuronal glucose oxidation are coupled during intense neuronal activation. *J Cereb Blood Flow Metab* 2004; 24: 972–985.
22. Logothetis NK, Pauls J, et al. Neurophysiological investigation of the basis of the fMRI signal. *Nature* 2001; 412: 150–157.
23. Viswanathan A and Freeman RD. Neurometabolic coupling in cerebral cortex reflects synaptic more than spiking activity. *Nat Neurosci* 2007; 10: 1308–1312.
24. Gordon GR, Choi HB, et al. Brain metabolism dictates the polarity of astrocyte control over arterioles. *Nature* 2008; 456: 745–749.
25. Volterra A and Meldolesi J. Astrocytes, from brain glue to communication elements: the revolution continues. *Nat Rev Neurosci* 2005; 6: 626–640.
26. Schummers J, Yu H and Sur M. Tuned responses of astrocytes and their influence on hemodynamic signals in the visual cortex. *Science* 2008; 320: 1638–1643.
27. Mangia S, Tkác I, et al. Sustained neuronal activation raises oxidative metabolism to a new steady-state level: evidence from ^{1}H NMR spectroscopy in the human visual cortex. *J Cereb Blood Flow Metab* 2007; 27: 1055–1063.
28. Eriksson G, Peterson A, et al. Sodium-dependent glutamate uptake as an activator of oxidative metabolism in primary astrocyte cultures from newborn rat. *Glia* 1995; 15: 152–156.
29. Cruz NF, Lasater A, et al. Activation of astrocytes in brain of conscious rats during acoustic stimulation: acetate utilization in working brain. *J Neurochem* 2005; 92: 934–947.
30. Dienel GA, Schmidt KC and Cruz NF. Astrocyte activation *in vivo* during graded photic stimulation. *J Neurochem* 2007; 103: 1506–1522.
31. Öz G, Berkich DA, et al. Neuroglial metabolism in the awake rat brain: CO_2 fixation increases with brain activity. *J Neurosci* 2004; 24: 11273–11279.
32. Schaller B, Mekle R, et al. Net increase of lactate and glutamate concentration in activated human visual cortex detected with magnetic resonance spectroscopy at 7 tesla. *J Neurosci Res* 2013; 91: 1076–1083.
33. Schaller B, Xin L, et al. Are glutamate and lactate increases ubiquitous to physiological activation?

A ^{1}H functional MR spectroscopy study during motor activation in human brain at 7Tesla. *Neuroimage* 2014; 93: 138–145.
34. Patel MS and Tilghman SM. Regulation of pyruvate metabolism via pyruvate carboxylase in rat brain mitochondria. *Biochem J* 1973; 132: 185–192.
35. Keech DB and Utter MF. Pyruvate Carboxylase: II. Properties. *J Biol Chem* 1963; 238: 2609–2614.
36. Kaufman EE and Driscoll BF. Carbon dioxide fixation in neuronal and astroglial cells in culture. *J Neurochem* 1992; 58: 258–262.
37. Qu H, Eloqayli H, et al. Glutamate decreases pyruvate carboxylase activity and spares glucose as energy substrate in cultured cerebellar astrocytes. *J Neurosci Res* 2001; 66: 1127–1132.
38. Patel AB, Chowdhury GMI, et al. Cerebral pyruvate carboxylase flux is unaltered during bicuculline-seizures. *J Neurosci Res* 2005; 79: 128–138.
39. Jackson JG, O'Donnell JC, et al. Neuronal activity and glutamate uptake decrease mitochondrial mobility in astrocytes and position mitochondria near glutamate transporters. *J Neurosci* 2014; 34: 1613–1624.
40. Xu S1, Yang J, et al. Metabolic alterations in focally activated primary somatosensory cortex of α-chloralose-anesthetized rats measured by ^{1}H MRS at 11.7 T. *Neuroimage* 2005; 28: 401–409.
41. Dienel GA. Brain lactate metabolism: the discoveries and the controversies. *J Cereb Blood Flow Metab* 2012; 32: 1107–1138.
42. Swanson RA, Morton MM, et al. Sensory stimulation induces local cerebral glycogenolysis: demonstration by autoradiography. *Neuroscience* 1992; 51: 451–461.
43. Harley CW, Milway JS and Fara-On M. Medial forebrain bundle stimulation in rats activates glycogen phosphorylase in layers 4, 5b and 6 of ipsilateral granular neocortex. *Brain Res* 1995; 685: 217–223.
44. Sickmann HM, Walls AB, et al. Functional significance of brain glycogen in sustaining glutamatergic neurotransmission. *J Neurochem* 2009; 109: 80–86.
45. Gibbs ME, Lloyd HG, et al. Glycogen is a preferred glutamate precursor during learning in 1-day-old chick: biochemical and behavioral evidence. *J Neurosci Res* 2007; 85: 3326–3333.